



Decadal evolution of aerosol-mediated ozone responses in Eastern China under clean air actions and carbon neutrality policies

Yasong Li^{1,3}, Chen Li², Yaoyu Li¹, Tijian Wang³, Mengmeng Li³, Yawei Qu⁴, Hao Wu⁵, Min Xie⁶, and
Yanjin Wang¹

¹College of Environmental Economics, Henan Finance University, Zhengzhou, 450046, China

²School of Energy and Chemical Engineering, Tianjin Renai College, Tianjin, 301636, China

³School of Atmospheric Sciences, Nanjing University, Nanjing, 210023, China

⁴College of Intelligent Science and Control Engineering,

Jinling Institute of Technology, Nanjing, 211112, China

⁵Key Laboratory of Transportation Meteorology of China Meteorological Administration,
Nanjing Joint Institute for Atmospheric Sciences, Nanjing, China

⁶School of Environment, Nanjing Normal University, Nanjing 210023, China

Correspondence: Tijian Wang (tjwang@nju.edu.cn)

Received: 19 August 2025 – Discussion started: 2 October 2025

Revised: 20 December 2025 – Accepted: 15 January 2026 – Published: 26 January 2026

Abstract. Despite substantial reductions in PM_{2.5} and other pollutants, ozone (O₃) in eastern China has increased over the past decade, yet the influence of aerosol processes – including aerosol–radiation interactions (ARI) and heterogeneous chemistry (HET) – on these trends remains insufficiently explored, particularly during Clean Air Action Plan (CAAP, Phase I: 2013–2017; Phase II: 2018–2020) and under carbon neutrality pathways. We applied a phase- and season-resolved WRF-Chem framework with explicit ARI and HET to quantify historical and projected O₃ changes in the Yangtze River Delta (YRD), linking aerosol effects with CAAP and carbon-neutrality pathways. We separate O₃ changes into those driven directly by anthropogenic emissions and meteorological variability, and those mediated by aerosol processes through ARI and HET. The results revealed that anthropogenic emissions and meteorological variability respectively dominated winter and summer O₃ increases. Winter O₃ increases were dominated by ARI: large aerosol reductions enhanced solar radiation, temperature, and photolysis, resulting in a photochemical O₃ rise (+1.14 (+0.74) ppb in Phase I (II)). Summer O₃ was more sensitive to HET. In Phase I, aerosol decreases weakened heterogeneous radical uptake, enhancing O₃ formation (+1.62 ppb). In Phase II, however, the net HET effect reversed sign (−2.86 ppb), driven by shifts in multiple heterogeneous pathways – including changes in radical uptake, HONO and N₂O₅ chemistry, and aerosol liquid water – rather than radical scavenging alone. Accounting for aerosol effects (AEs = ARI + HET), reductions in PM_{2.5} and NO_x increased O₃, while VOCs reductions consistently lowered O₃ in both seasons. Under carbon peaking and neutrality scenarios with AEs, winter O₃ increased by 6.7 % and 10.7 %, whereas summer O₃ decreased by 2.9 % and 6.7 %, highlighting seasonally contrasting responses. These results underscore the necessity of explicitly accounting for multi-path aerosol–O₃ interactions in both near-term air quality management and long-term climate mitigation to prevent unintended trade-offs and maximize co-benefits.

1 Introduction

Over the last decade, a series of landmark policy initiatives – such as the Air Pollution Prevention and Control Action Plan (Phase I: 2013–2017), the Three-Year Blue Sky Protection Campaign (Phase II: 2018–2020), and the subsequent dual-carbon strategy – have driven substantial and persistent declines in $\text{PM}_{2.5}$ concentrations across China's major urban clusters (Geng et al., 2024; Zhai et al., 2019). However, in sharp contrast to these successes, ground-level O_3 have continued to rise, particularly in economically developed regions such as Beijing-Tianjin-Hebei (BTH, Zhao et al., 2023; Dai et al., 2023), the Yangtze River Delta (YRD, Li et al., 2023; Hu et al., 2025), and the Pearl River Delta (PRD, Chen et al., 2020). For example, Yan et al. (2024) reported that the annual mean maximum daily 8 h average (MDA8) O_3 in major Chinese cities increased from $106.0 \mu\text{g m}^{-3}$ in 2013 to $131.1 \mu\text{g m}^{-3}$ in 2022, with the most pronounced growth observed in the BTH and YRD regions. The emerging decoupling between $\text{PM}_{2.5}$ and O_3 trends underscores the growing complexity of air pollution control in China, suggesting that conventional precursor-oriented mitigation strategies may be insufficient to address secondary pollutants formed through nonlinear atmospheric processes. The increasing frequency and intensity of O_3 pollution episodes not only pose serious risks to human health and ecosystems (Liu et al., 2018; Li et al., 2020b) but also diminish the co-benefits of $\text{PM}_{2.5}$ mitigation. As China advances toward its goal of carbon neutrality, elucidating the mechanisms behind this counterintuitive O_3 rise has become both a scientific imperative and a policy priority.

Extensive research has identified anthropogenic emissions and meteorological variability as the two dominant drivers of observed O_3 increases (Ma et al., 2023a; Sun et al., 2019; Shao et al., 2024; Ni et al., 2024), particularly during the early stages of the CAAP. For instance, Dang et al. (2021) used the GEOS-Chem model to show that during the summer of 2012–2017, meteorological changes accounted for 49 % of the O_3 increase in the BTH region and 84 % in the YRD, while emission changes explained 39 % and 13 %, respectively. Recent efforts combining numerical modeling with machine learning have further highlighted the critical roles of solar radiation and temperature, especially during the COVID-19 lockdown. Zhang et al. (2025) attributed approximately 94 % of the summer O_3 increase in the Hangzhou Bay area from 2019 to 2022 to meteorological influences, noting a growing dominance of meteorological drivers over emission-related factors. In addition, innovative metrics such as the O_3 -specific emission–meteorology index (EMI/ O_3) have been proposed to quantify these contributions, revealing that summer O_3 increases in cities like Beijing and Shanghai were largely governed by volatile organic compound (VOCs) emissions and meteorological shifts (Lu et al., 2025).

Beyond emissions and meteorology, aerosol effects (AEs) have emerged as important, though often overlooked, reg-

ulators of surface O_3 . Aerosols influence O_3 formation through two principal mechanisms: aerosol–radiation interaction (ARI), which alter photolysis rates and boundary layer dynamics, and heterogeneous chemistry (HET), which removes hydroperoxyl (HO_2) radical and suppresses O_3 formation (Li et al., 2025, 2024b, 2019a; Gao et al., 2018). As aerosol loading has substantially declined under clean air policies, the magnitudes and directions of these mechanisms may have shifted. For instance, Yu et al. (2019) found that reductions in $\text{PM}_{2.5}$ contributed to approximately 22 % of the observed O_3 increase in the YRD during 2013–2017. Yang et al. (2024) quantified a 0.81 ppb increase in summer O_3 linked to the weakening of ARI under lower aerosol conditions. Previous analyses indicated that diminished aerosol modulation of photochemistry through ARI, photolysis rate suppression, and heterogeneous reactions jointly contributed to a 22.2 %–57.3 % enhancement in O_3 growth between 2014 and 2020 (Li et al., 2024a). Similarly, Liu et al. (2023a) identified weakened HET as the dominant mechanism behind O_3 increases across both phases of the CAAP. Moreover, precursor– O_3 relationships are strongly modulated by background aerosol levels, further emphasizing the need to assess O_3 responses under evolving aerosol conditions to ensure the effectiveness of co-control strategies. Anthropogenic emissions and meteorological variability act as external drivers that directly regulate precursor concentrations, atmospheric chemical regimes, and transport processes. In contrast, ARI and HET represent aerosol-mediated mechanisms that reshape the photochemical environment by altering photolysis rates and radical budgets. These aerosol-driven mechanisms determine the extent to which surface O_3 responds to precursor (particularly NO_x) reductions or meteorological perturbations. This conceptual framework underpins our separation of O_3 changes into externally driven components and aerosol-modulated components in this study.

Despite increasing recognition of the role of aerosols in modulating surface O_3 , several critical knowledge gaps remain. Most existing studies tend to isolate either ARI or HET rather than evaluate their combined and potentially synergistic effects. Additionally, few investigations adopt a phase- and season-resolved framework aligned with policy implementation timelines, and even fewer consider long-term projections under carbon neutrality pathways. Furthermore, the spatial heterogeneity and nonlinear chemical responses of O_3 under dynamic aerosol environments remain poorly characterized, particularly in densely populated and industrialized regions like the YRD. To address these gaps, this study employs an improved WRF-Chem modeling framework to conduct a comprehensive, phase-, season-, and mechanism-resolved assessment of AEs in the YRD from 2013 to 2024. By explicitly disentangling the effects of ARI and HET and integrating them with historical emission changes, meteorological variability, and future carbon neutrality–driven mitigation scenarios, we aim to systematically quantify the drivers of past O_3 trends and predict their future trajectory.

ries. Furthermore, we assessed the responses of O_3 to reductions in individual precursors ($PM_{2.5}$, NO_x , VOCs, NH_3 , and SO_2), thereby elucidating the conditions under which synergistic air quality and climate co-benefits can be most effectively realized. These results provide a scientific basis for the development of region-specific and seasonally adaptive O_3 mitigation strategies that are consistent with China's dual objectives of air pollution control and carbon neutrality.

2 Methodology

2.1 Model and dataset

To diagnose the mechanisms governing surface O_3 variability over eastern China under the Clean Air Action Plan (CAAP), we applied an improved configuration of the Weather Research and Forecasting model coupled with Chemistry (WRF-Chem, version 3.7.1, Grell et al., 2005). The analysis focused on two major implementation stages of the CAAP (Phase I and Phase II), with the objective of disentangling the relative contributions of emission controls, meteorological variability, and aerosol-mediated processes to long-term O_3 changes. Particular attention was devoted to two key aerosol effects (ARI and HET) and their roles in modulating O_3 trends. In addition, sensitivity experiments were conducted to quantify O_3 responses to precursor emission reductions, and to evaluate future surface O_3 behavior under carbon neutrality-oriented emission pathways while explicitly accounting for combined aerosol effects (ARI + HET). Building upon our previous modeling framework, the WRF-Chem setup largely followed configurations documented in earlier studies (Li et al., 2024a, b), with targeted enhancements to address the objectives of this work. A three-tier nested domain system was implemented, encompassing East Asia as the outermost domain, eastern China as the intermediate domain, and the YRD as the innermost domain (Fig. S1 in the Supplement). Biogenic emissions were calculated online using the Model of Emissions of Gases and Aerosols from Nature (Guenther et al., 2006). Numerical simulations were performed for January and July to characterize representative winter and summer conditions, respectively. Each seasonal simulation covered a five-week period (29 December to 1 February for winter, and 28 June to 1 August for summer), with the initial three days excluded to allow for model spin-up and chemical equilibration. Beyond the seasonal analyses, the decadal evolution of maximum daily 8 h average (MDA8) O_3 over the YRD during 2013–2024 was systematically examined for both seasons. Detailed information about the spatial distribution and technical characteristics of the monitoring stations and model configuration have been reported in our previous studies (Li et al., 2024a).

2.2 Aerosol effects enhancement

This work provided a comprehensive evaluation of aerosol-mediated influences on surface O_3 variability within the dual context of China's CAAP and prospective carbon neutrality pathways. Two representative aerosol-related processes (ARI and HET) were explicitly represented in the WRF-Chem modeling system to account for the coupled physical and chemical pathways through which aerosols regulate O_3 formation. The formulation, implementation, and performance evaluation of these processes followed the methodologies established in our earlier studies and are only briefly outlined here for completeness (Li et al., 2024b). Within this framework, ARI modulated O_3 concentrations through two primary mechanisms. First, aerosols attenuated incoming solar radiation, thereby influencing photolysis frequencies through light extinction. Second, aerosols perturbed meteorological conditions by altering radiative fluxes, giving rise to aerosol–radiation feedbacks (ARF). While ARF was natively supported in the standard WRF-Chem configuration, the default Fast-J photolysis scheme did not dynamically account for aerosol optical properties, which led to the omission of aerosol extinction effects on photolysis rates. To overcome this deficiency, a customized coupling interface was implemented to link prognostic aerosol optical parameters – such as scattering and absorption coefficients – to the Fast-J module. This modification allowed aerosol optical depth to be calculated online and enabled photolysis rates to respond consistently to the evolving spatial and temporal distributions of aerosols.

Heterogeneous chemistry exerts complex influences on O_3 formation by altering radical budgets, modifying reactive nitrogen cycling, and changing aerosol-phase reaction rates. In the enhanced WRF-Chem, HET is represented through multiple pathways on dust and black carbon surfaces, including (1) heterogeneous uptake of HO_2 , OH , NO_2 , and NO_3 ; (2) nighttime N_2O_5 hydrolysis to $2HNO_3$; (3) heterogeneous formation of $HONO$ from NO_2 uptake on carbonaceous aerosols; (4) SO_2 and H_2SO_4 heterogeneous oxidation; and (5) direct O_3 uptake on dust and black carbon surfaces. These processes collectively modify photolysis-driven radical initiation and NO_x partitioning. Therefore, the net HET effect reflects the balance among several aerosol-mediated pathways rather than a single mechanism. The heterogeneous reactions considered in this study, together with their corresponding uptake coefficients (γ), were summarized in Table S1 in the Supplement. Key parameters, including uptake coefficients, aerosol surface area densities, and photolysis scaling factors, followed values that had been validated in our previous modeling studies (Li et al., 2024b). The enhanced WRF-Chem system had been systematically assessed in earlier work and was demonstrated to realistically reproduce meteorological fields, aerosol characteristics, and trace gas concentrations in China, with particularly robust performance in YRD (Qu et al., 2023; Li et al., 2018).

2.3 Numerical experimental designs

To disentangle the respective and combined influences of anthropogenic emission changes, meteorological variability, and aerosol-related processes on surface O₃, three groups of numerical experiments were designed within the enhanced WRF-Chem modeling framework (Table 1).

2.3.1 (1) SET1: Historical Attribution Simulations (2013–2020)

The first set of simulations was conducted to identify the dominant drivers of O₃ variability during two major stages of CAAP, referred to as Phase I and Phase II. In total, 11 simulations were performed to isolate the effects of emission changes, meteorological variability, and aerosol-related mechanisms. To quantify the impact of anthropogenic emission changes alone, three simulations were conducted using fixed meteorological conditions from 2020, with all aerosol-related effects disabled (13E20M_NOALL, 17E20M_NOALL, and 20E20M_NOALL). Differences among these simulations represented the net O₃ response to emission evolution in the absence of aerosol feedbacks and meteorological variability. The contribution of meteorological variability was assessed through an additional set of simulations using fixed anthropogenic emissions from 2013 while varying meteorological conditions (2013, 2017, and 2020). Aerosol-related processes were excluded in these runs (13E13M_NOALL, 13E17M_NOALL, and 13E20M_NOALL), and the resulting differences quantified the meteorology-driven component of O₃ changes. To evaluate aerosol effects (AEs), three parallel simulations were conducted for each emission year (2013, 2017, and 2020): (i) with all aerosol-related processes enabled (AEs), (ii) with heterogeneous chemistry disabled (NOHET), and (iii) with all aerosol effects turned off (NOALL). Pairwise comparisons among these simulations (e.g., AEs-NOHET, NOHET-NOALL, and AEs-NOALL) allowed the individual contributions of heterogeneous chemistry (HET), aerosol–radiation interactions (ARI), and their combined effects to be quantified. For example, the difference between 20E20M_AEs and 20E20M_NOHET isolated the HET contribution under 2020 emission conditions, whereas the comparison between 20E20M_NOHET and 20E20M_NOALL represented the ARI effect. This analytical framework was applied consistently across all emission years to characterize phase-resolved aerosol influences on O₃ trends. A schematic illustration of the experimental design and the associated O₃ responses was provided in Fig. 1.

2.3.2 (2) SET2: Single-Precursor Sensitivity Experiments (2020 baseline)

The second group of simulations was designed to examine the nonlinear responses of O₃ to individual precursor emission controls under active aerosol effects. All experiments

were based on the 2020 anthropogenic emissions inventory. For each simulation, emissions of one precursor (primary PM_{2.5}, NO_x, volatile organic compounds (VOCs), SO₂, or NH₃) were reduced by 25 % and 50 %, while emissions of the remaining species were held constant. Reductions in primary PM_{2.5} included both black carbon (BC) and organic carbon (OC).

2.3.3 (3) SET3: Multi-Pollutant Co-Reduction Experiments (Future Scenarios)

The third set of experiments explored potential O₃ responses under future emission mitigation pathways aligned with China's carbon peaking and carbon neutrality objectives. Coordinated reductions in all major anthropogenic emissions were applied, guided by the mid- and long-term projections reported by Cheng et al. (2021), who assessed China's air quality evolution under dual-carbon strategies. Their analysis suggested that anthropogenic emissions will decrease by approximately 26 %–32 % by 2030 relative to 2020 levels, followed by a slower reduction pace thereafter, reaching a maximum decline of about 31 % by 2060 compared to 2030. Based on these projections, two representative reduction levels – 30 % and 50 % – were selected to approximate emission conditions corresponding to the carbon peaking (2030) and carbon neutrality (2060) targets, respectively. To further characterize the nonlinear O₃ response under increasingly stringent mitigation, a series of additional co-control scenarios spanning 10 %, 20 %, 40 %, 60 %, 70 %, 80 %, and 90 % reductions was implemented. Across all future experiments, emissions of primary PM_{2.5}, NO_x, VOCs, SO₂, and NH₃ were scaled down proportionally, reflecting a coordinated multi-pollutant mitigation framework. Aerosol-related processes were consistently enabled in all simulations to preserve realistic aerosol–O₃ feedbacks.

2.4 Historical changes in emissions and observed O₃

Interannual changes in six key species – SO₂, primary PM_{2.5}, BC, OC, NO_x, and VOCs – at the provincial scale in the YRD during 2013–2020 was presented in Fig. S2. Over this period, emissions of most pollutants declined substantially, with the exception of VOCs. Cumulatively, SO₂, primary PM_{2.5}, BC, OC, and NO_x emissions were reduced by 69.7 %, 46.9 %, 40.4 %, 38.0 %, and 27.9 %, respectively. During the first phase of the CAAP (Phase I), control strategies were predominantly oriented toward particulate matter abatement. As a result, primary PM_{2.5}, BC, and OC emissions decreased markedly by 37.0 %, 30.0 %, and 27.3 %, respectively. Concurrently, notable reductions were achieved for major gaseous precursors, with SO₂ and NO_x declining by 56.4 % and 19.8 %. In contrast, the absence of explicit VOCs-targeted measures during this stage led to a 7.1 % increase in VOCs emissions (Li et al., 2019b). The second phase of the CAAP (Phase II) was characterized by a

Table 1. Overview of WRF-Chem numerical experiments.

Scenario sets	Scenario ID	Anthropogenic emissions	Meteorology	HET ^a	ARI ^b
SET1	20E20M_AEs			✓	✓
	20E20M_NOHET	2020		✗	✓
	20E20M_NOALL			✗	✗
	17E20M_AEs			✓	✓
	17E20M_NOHET	2017	2020	✗	✓
	17E20M_NOALL			✗	✗
	13E20M_AEs			✓	✓
	13E20M_NOHET	2013		✗	✓
	13E20M_NOALL			✗	✗
	13E13M_NOALL	2013	2013	✗	✗
	13E17M_NOALL	2013	2017	✗	✗
SET2	CUT_PM2.5_25/50	25 (50) % reduction in PM _{2.5} in 2020			
	CUT_NO _x _25/50	25 (50) % reduction in NO _x in 2020			
	CUT_VOCs_25/50	25 (50) % reduction in VOCs in 2020			
	CUT_NH ₃ _25/50	25 (50) % reduction in NH ₃ in 2020			
	CUT_SO ₂ _25/50	25 (50) % reduction in SO ₂ in 2020			
SET3	CUT_MEIC_10	10 % reduction in 2020	2020	✓	✓
	CUT_MEIC_20	20 % reduction in 2020			
	CUT_MEIC_30	30 % reduction in 2020			
	CUT_MEIC_40	40 % reduction in 2020			
	CUT_MEIC_50	50 % reduction in 2020			
	CUT_MEIC_60	60 % reduction in 2020			
	CUT_MEIC_70	70 % reduction in 2020			
	CUT_MEIC_80	80 % reduction in 2020			
	CUT_MEIC_90	90 % reduction in 2020			

HET^a: Heterogeneous chemistry (HET) was activated by setting the heterogeneous reaction switch to 1.

ARI^b: Aerosol–radiation interaction (ARI) was activated by turning on the aerosol–radiation feedback (aer_ra_feedback = 1) and by linking aerosol optical properties to the photolysis calculation.

transition toward more coordinated regulation of NO_x and VOCs. Although emissions of SO₂, NO_x, and PM_{2.5} continued to decrease, the overall pace of reduction was slower than that observed in Phase I. Specifically, NO_x and VOCs emissions declined by 7.4 % and 4.6 %, respectively. Nevertheless, when considering the entire 2013–2020 period, VOCs emissions in the YRD still exhibited a net increase of 2.2 %. From a spatial perspective, emission reductions were most pronounced in the northwestern and central subregions of the YRD (Fig. S3), a pattern that aligns with national emission reduction trends and is consistent with previous regional assessments (Liu et al., 2023a; Yan et al., 2024).

In addition to modifying emissions, the CAAP brought about substantial changes in observed O₃. Figure 2 illustrated the annual variation of the MDA8 O₃ in winter and summer across the YRD based on ground-based observations from 2013 to 2024. In winter, O₃ increased by approximately 7 µg m⁻³ during 2013–2017, at an average annual growth rate of 3 %. This trend reversed during 2017–2020, with a decrease of 4 µg m⁻³ (2 % yr⁻¹), followed by a modest increase of 2.2 µg m⁻³ (0.91 % yr⁻¹) between 2020 and 2024. In summer, O₃ rose by 13.2 µg m⁻³ during 2013–2017, con-

tinued to increase by 4.9 µg m⁻³ from 2017 to 2020, and then declined sharply by 11.4 µg m⁻³ during 2020–2024. These results suggested that in the early phase of clean air efforts, the insufficient control of O₃ precursors contributed to significant increases in both winter and summer O₃. However, stronger VOCs and NO_x control measures in recent years appeared to mitigate this upward trend. A particularly sharp drop in O₃ between 2020 and 2021 was likely caused by a combination of intensified emission reductions and unusual meteorological conditions (Yin et al., 2021). Overall, observed MDA8 O₃ in the YRD increased by 12.1 % in winter and 11.8 % in summer during 2013–2017. In the subsequent periods (2017–2020 and 2020–2024), winter O₃ levels first declined and then rebounded, while summer O₃ initially rose and then decreased. The underlying causes of these contrasting patterns were explored in detail in the Results section. Note that this study did not focus on the spatial distribution of O₃ changes, as this topic has already been extensively examined in previous literature (Hu et al., 2025; Zhao et al., 2023).

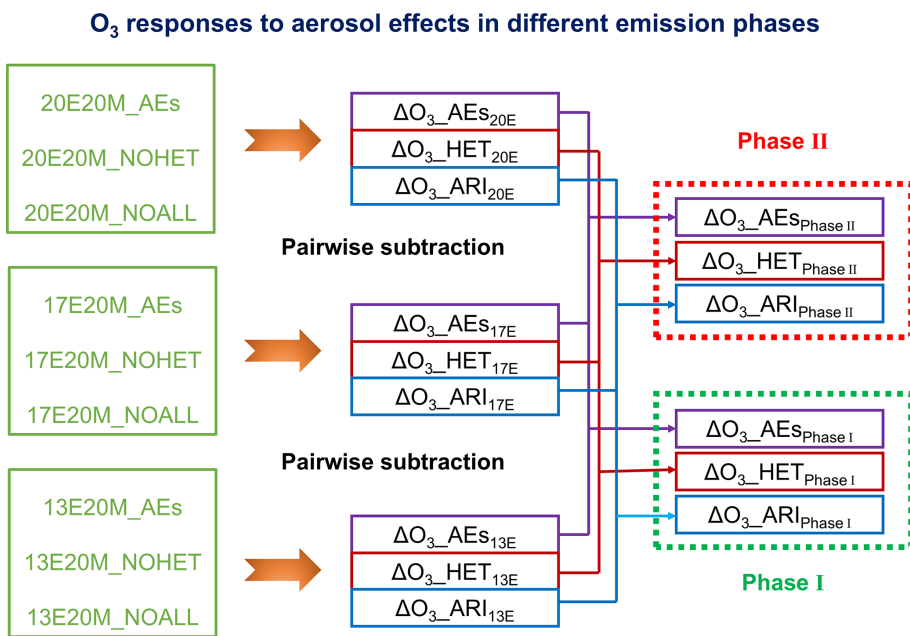


Figure 1. Conceptual diagram illustrating the scenario design and the associated ozone responses to aerosol-mediated processes during the CAAP phases. Note: HET = heterogeneous chemistry, ARI = aerosol-radiation interaction, AEs = aerosol effects (HET + ARI). Scenario IDs such as “13E20M” refer to emission year 2013 with 2020 meteorology.

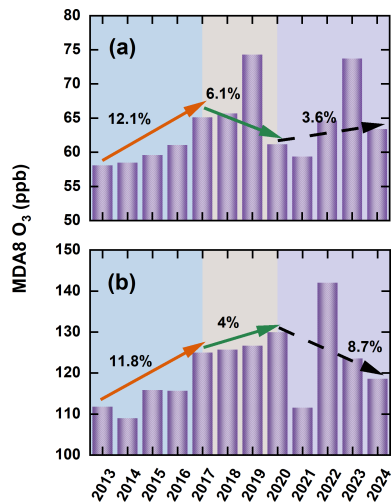


Figure 2. Interannual variations in winter (a) and summer (b) MDA8 O₃ concentrations (ppb) across the YRD during 2013–2024, derived from continuous ground-based measurements.

3 Results and discussion

The accuracy of simulated meteorological parameters and pollutant concentrations under scenario (20E20M_AEs) has been thoroughly validated against ground-based observations in earlier work (Li et al., 2024a). As summarized in Table S2, the model reasonably captures the magnitude, seasonal variability of PM_{2.5}, O₃, as well as the major features of tempera-

ture, relative humidity, and wind speed. These results provide confidence in the model's ability to represent the atmospheric conditions relevant to the subsequent analysis.

3.1 Attribution of historical seasonal O₃ changes to emissions and meteorology

A set of attribution simulations (SET1) with aerosol processes disabled (NOALL) and fixed 2020 meteorology was conducted to isolate emission-driven O₃ variability in the YRD over the past decade, with the resulting responses shown in Fig. 3. During Phase I, emission reductions unexpectedly led to O₃ increases of 6.3 ppb in winter and 1.3 ppb in summer. In contrast, Phase II witnessed coordinated NO_x and VOCs controls, leading to O₃ reductions of 0.9 ppb (winter) and 1.5 ppb (summer). These contrasting outcomes reflect the nonlinear chemistry of O₃ formation. While Phase I focused primarily on reducing PM_{2.5} and SO₂, VOCs emissions remained poorly regulated and even increased, enhancing photochemical activity. In contrast, Phase II adopted a more balanced control strategy targeting both NO_x and VOCs, which proved more effective in mitigating O₃ pollution. Spatially, the strongest O₃ responses occurred in the northwestern and central parts of the YRD, aligning with regions that experienced the largest emission reductions.

To assess the influence of meteorological conditions, we fixed anthropogenic emissions at 2013 levels and varied the meteorological fields across years. Results revealed seasonally asymmetric impacts: meteorology contributed to winter-time O₃ declines (1.7 and 2.1 ppb during Phases I and II,

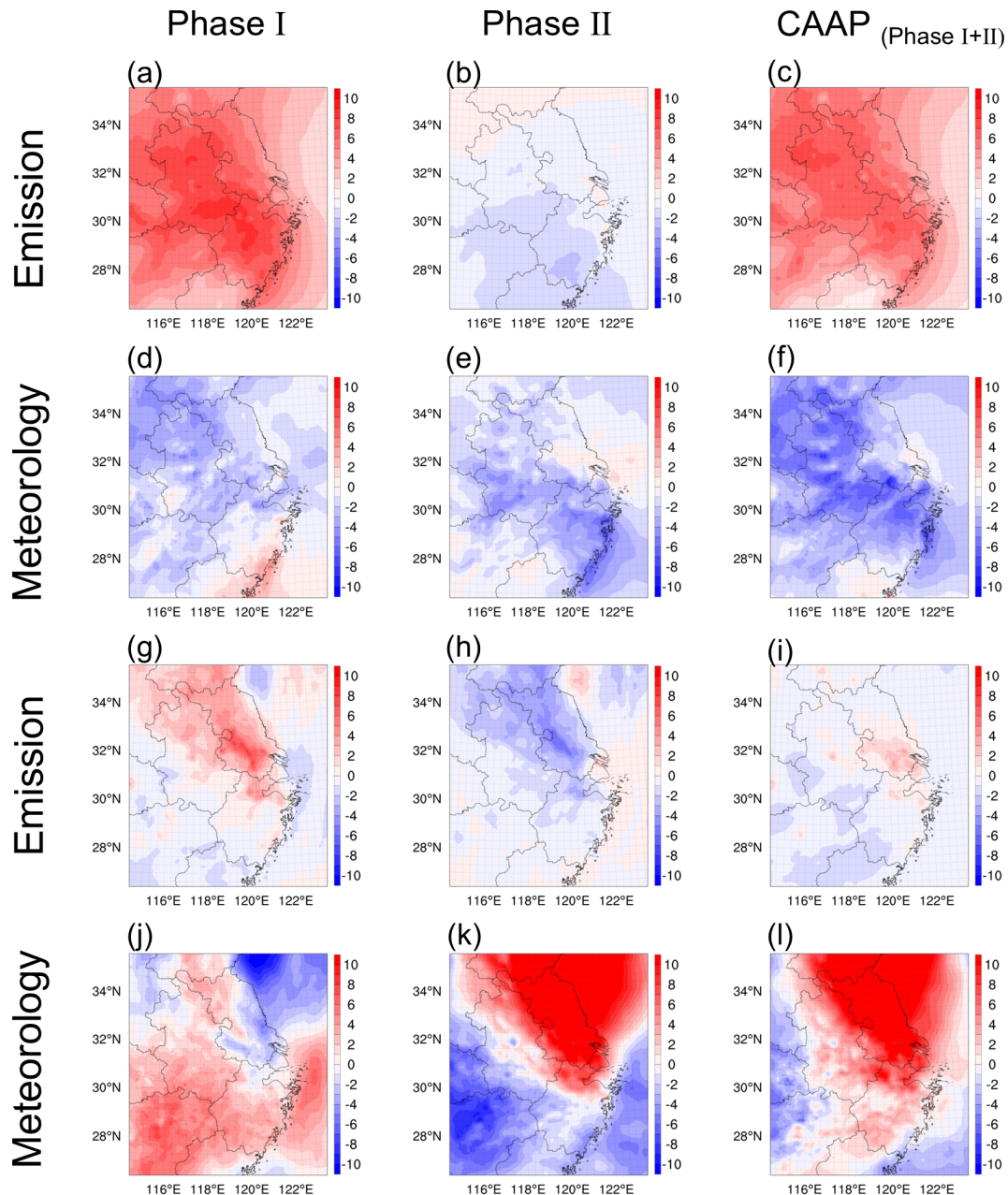


Figure 3. Attribution of seasonal O₃ variations (ppb) in the Yangtze River Delta to emission reductions (a–c, g–i) and meteorological influences (d–f, j–l) during Phase I and Phase II of the CAAP, with winter and summer results displayed in the upper and lower rows, respectively.

respectively), but promoted summertime O₃ increases (1.4 and 4.6 ppb). This highlighted a distinct seasonal asymmetry in meteorological influences on O₃. As summarized in Table S3, changes in five key meteorological parameters (shortwave radiation (SW), temperature (T₂), relative humidity (RH₂), planetary boundary layer height (PBLH), and wind speed (WS₁₀)) collectively explain these trends. In winter, lower radiation and T₂, higher RH₂, and stronger WS₁₀ suppressed O₃ formation and accumulation. Conversely, sum-

mer conditions characterized by higher radiation and T₂, coupled with lower RH₂ and weaker WS₁₀, favored O₃ build-up. Although this study does not explicitly quantify the relative contributions of individual meteorological factors, prior studies (Liu et al., 2023a; Yan et al., 2024; Dai et al., 2024) using multiple linear regression consistently identify SW and T₂ as dominant drivers. Figure S4 presented the spatial distributions of meteorological changes during 2013–2020, revealing that the most pronounced shifts – especially in radiation

and temperature-occurred in the central YRD and were more significant in summer, consistent with stronger O₃ responses.

In summary, anthropogenic emission changes were the dominant drivers of winter O₃ increases during Phase I. These findings are consistent with earlier research (Cao et al., 2022; Wu et al., 2022), which similarly highlighted that early-phase air quality interventions—though effective in reducing PM_{2.5}—often overlooked the complex chemistry of O₃, particularly the roles of VOCs and NO_x, thereby unintentionally intensifying O₃ pollution. The transition to coordinated multi-pollutant control strategies in Phase II enabled more effective O₃ mitigation. In addition, the role of meteorology was non-negligible. Our findings, in line with those of Liu and Wang (2020), emphasize a pronounced seasonal asymmetry—meteorology suppressed winter O₃ but enhanced summer levels. Notably, wintertime O₃ variability was primarily emission-driven during Phase I, but increasingly influenced by meteorology in Phase II. In contrast, summer O₃ changes were consistently dominated by meteorological variability across both phases. These insights underscore the need for future O₃ control strategies to account for both emissions and meteorological variability, particularly in the context of climate change and evolving pollution regimes. These externally driven O₃ changes provide the foundation for evaluating how aerosol-mediated processes further modulate the emission-driven portion of the O₃ response.

3.2 Aerosol multi-effects contributions to past seasonal O₃ variations

Building on the external drivers identified in Sect. 3.1, we next examined how ARI and HET modified the emission-reduction-driven O₃ response. Figure 4 illustrated the wintertime spatial patterns of O₃ changes driven by ARI and HET across the YRD during both phases of the CAAP. In Phase I, ARI induced a significant O₃ increase of up to 1.14 ppb across the region, while the contribution from HET was notably smaller at 0.32 ppb. This indicated that early aerosol reductions primarily enhanced O₃ via increased solar radiation and associated meteorological feedbacks, rather than through the suppression of radical uptake on particle surfaces. This finding contrasted with those of Li et al. (2019a), who—using GEOS-Chem simulations—attributed O₃ increases over the BTH to reduced HO₂ uptake under declining PM_{2.5}. The discrepancy may stem from differences in model representation; our framework explicitly incorporates both ARI-driven meteorological feedbacks and the direct photolysis attenuation by aerosols, enabling a more comprehensive simulation of aerosol–radiation interaction. During Phase II, the ARI-induced O₃ increase weakened to +0.74 ppb, and the contribution from HET became negligible or slightly negative (−0.01 ppb). This suggested that ARI remained the dominant aerosol-related driver of winter O₃ variability, while the influence of HET diminished. The reduced overall aerosol impact during this phase was consistent with smaller pri-

mary PM_{2.5} emission reductions (−8 % in Phase II compared to −37 % in Phase I). Summing the contributions from both mechanisms, the total aerosol-driven O₃ enhancement reached +1.46 ppb in Phase I and +0.73 ppb in Phase II, culminating in a net wintertime increase of +2.2 ppb over the CAAP period.

In contrast to winter, summertime O₃ responses to AEs revealed different dominant mechanisms and magnitudes, as shown in Fig. 5. In Phase I, HET played a more substantial role, contributing a 1.62 ppb increase, whereas ARI slightly suppressed O₃ by 0.51 ppb. This pattern indicated that under high photochemical activity, reduced particulate matter significantly weakened radical scavenging, thereby elevating HO₂ levels and promoting O₃ formation. During Phase II, however, HET unexpectedly contributed a 2.86 ppb decrease in O₃, while ARI induced a 1.56 ppb enhancement. The HET-driven decrease may be linked to complex nonlinear chemical responses under further reduced aerosol backgrounds, which diminished the amplification effect of radical availability. Across both phases, HET consistently emerged as the primary driver of summertime aerosol-related O₃ variability. When aggregated, aerosols contributed a 1.11 ppb increase in Phase I and a 1.30 ppb decrease in Phase II, yielding a modest net summer reduction of 0.19 ppb over the CAAP period.

To elucidate the underlying mechanisms of aerosol impacts on O₃, we examined the changes in key meteorological variables, photolysis rates, and HO₂ radical concentrations induced by ARI and HET during the two implementation phases of the CAAP. Figure 6 presented the variations in five key meteorological parameters and the NO₂ photolysis rate (J_{NO_2}) in winter and summer as influenced by ARI. The results indicated that ARI consistently enhanced J_{NO_2} , SW, T_2 , WS₁₀, and PBLH, while reducing RH₂ during winter across both phases. These modifications—especially increased SW and T_2 —significantly facilitated photochemical O₃ production, thereby elevating O₃. Notably, the magnitude of these changes was substantially greater in Phase I than in Phase II, which can be attributed to the more pronounced reductions in aerosol emissions during the earlier phase. In summer, ARI and HET exerted contrasting influences on ground-level O₃, with their effects reversing between the two phases. ARI led to a slight decrease in O₃ (−0.51 ppb), likely due to enhanced vertical mixing from reduced aerosol extinction, which increased solar radiation and photolysis rates. However, the concurrent rise in temperature and PBLH may have diluted surface O₃ in certain regions (Fig. 6b), resulting in a net negative O₃ response to ARI during this phase. In Phase II, the ARI-induced increases in T_2 and photolysis rates more effectively enhanced photochemical O₃ production. Simultaneously, reductions in PBLH and WS₁₀ during this period suppressed vertical and horizontal O₃ dispersion (Fig. 6b), collectively leading to a net positive O₃ response (+1.56 ppb).

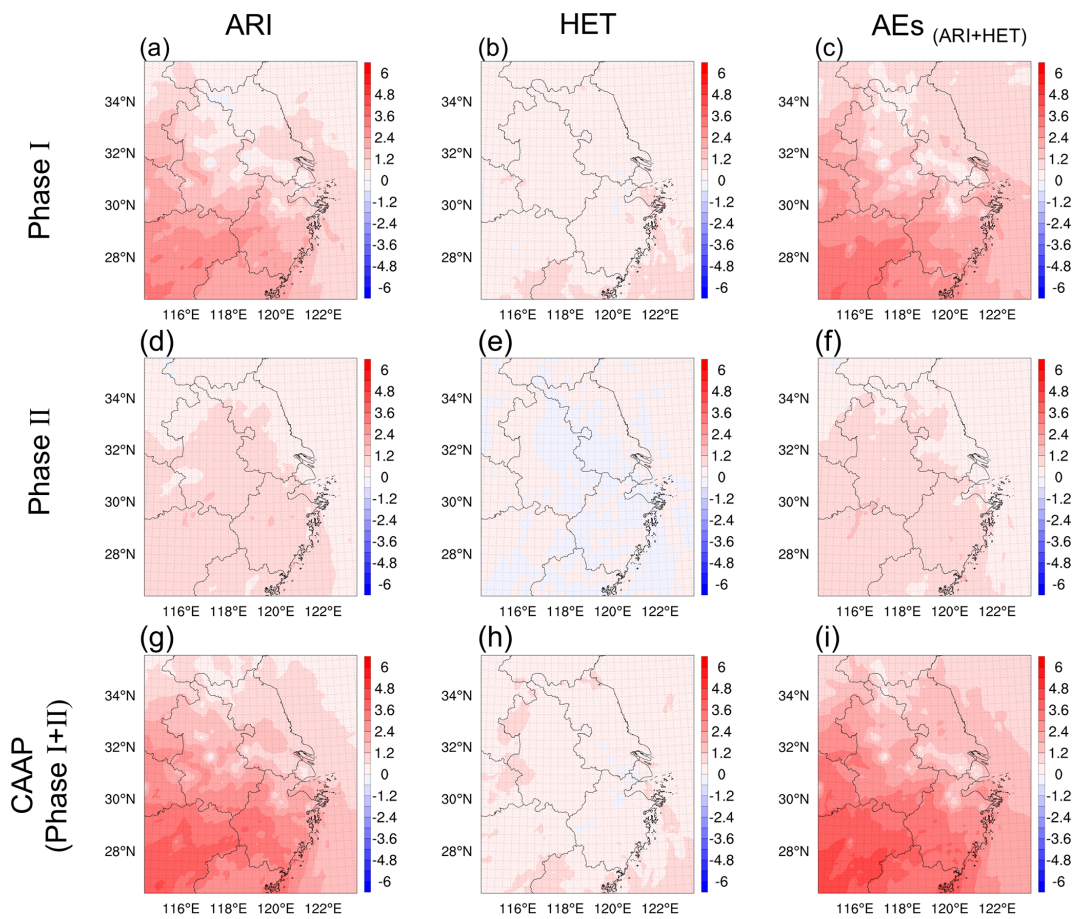


Figure 4. Spatial distribution of winter O₃ changes (ppb) over YRD driven by ARI (a, d, g), HET (b, e, h) and their combined effects (AEs, c, f, i) during two stages of the CAAP.

During Phase I, the substantial reductions in aerosol mass and surface area primarily weakened HO₂ heterogeneous uptake, as indicated by elevated HO₂ (Fig. 7d). This reduction in radical loss increased the availability of HO₂ and OH, leading to an enhancement in the photochemical ozone production term $P(O_3)$ (Dyson et al., 2023). In parallel, N₂O₅ also increased during Phase I (Fig. S5a), consistent with suppressed heterogeneous hydrolysis under reduced aerosol liquid water (ALW) and diminished aerosol surface area (Brown and Stutz, 2012). The weakened N₂O₅ hydrolysis further limited nighttime conversion of reactive nitrogen to HNO₃, maintaining NO_x in more photochemically active forms (Ma et al., 2023b). Meanwhile, heterogeneous NO₂ uptake – an important HONO source – was significantly reduced, consistent with the simulated decrease in HONO (Fig. S5d). The reduction in HONO slightly weakened early-morning radical initiation (Yu et al., 2022), but this influence was outweighed by the strong enhancement in HO₂ and the limited conversion of NO_x into HNO₃. As a result, HET exerted a net positive contribution to O₃ (+1.62 ppb) in Phase I. In contrast, Phase II exhibited a fundamentally different chemical response. Although aerosol loadings con-

tinued to decrease, the relative importance of heterogeneous pathways shifted substantially. HO₂ declined during Phase II (Fig. 7e), indicating a reduced radical pool and weaker propagation of daytime photochemical production. At the same time, N₂O₅ decreased markedly (Fig. S5b), suggesting that nighttime NO₃/N₂O₅ chemistry became less effective at sustaining reactive nitrogen cycling under even lower aerosol surface area and ALW. Rather than promoting efficient nighttime NO_x recycling, this suppression favored a net loss of reactive nitrogen through terminal sinks (e.g., HNO₃), shifting NO_x partitioning toward less photochemically active forms and weakening daytime $P(O_3)$. Conversely, HONO concentrations rebounded during Phase II (Fig. S5e). This increase reflects the altered balance between NO₂ uptake and nighttime NO_x partitioning under reduced N₂O₅ hydrolysis. However, despite this HONO increase, its positive effect on radical initiation could not compensate for the combined decline in HO₂, weakened N₂O₅ hydrolysis, and enhanced HNO₃ formation (George et al., 2015). The joint effect was a net reduction in the morning radical pool and diminished photochemical O₃ production (−2.86 ppb). This multi-pathway adjustment explains the observed sign reversal of HET's ef-

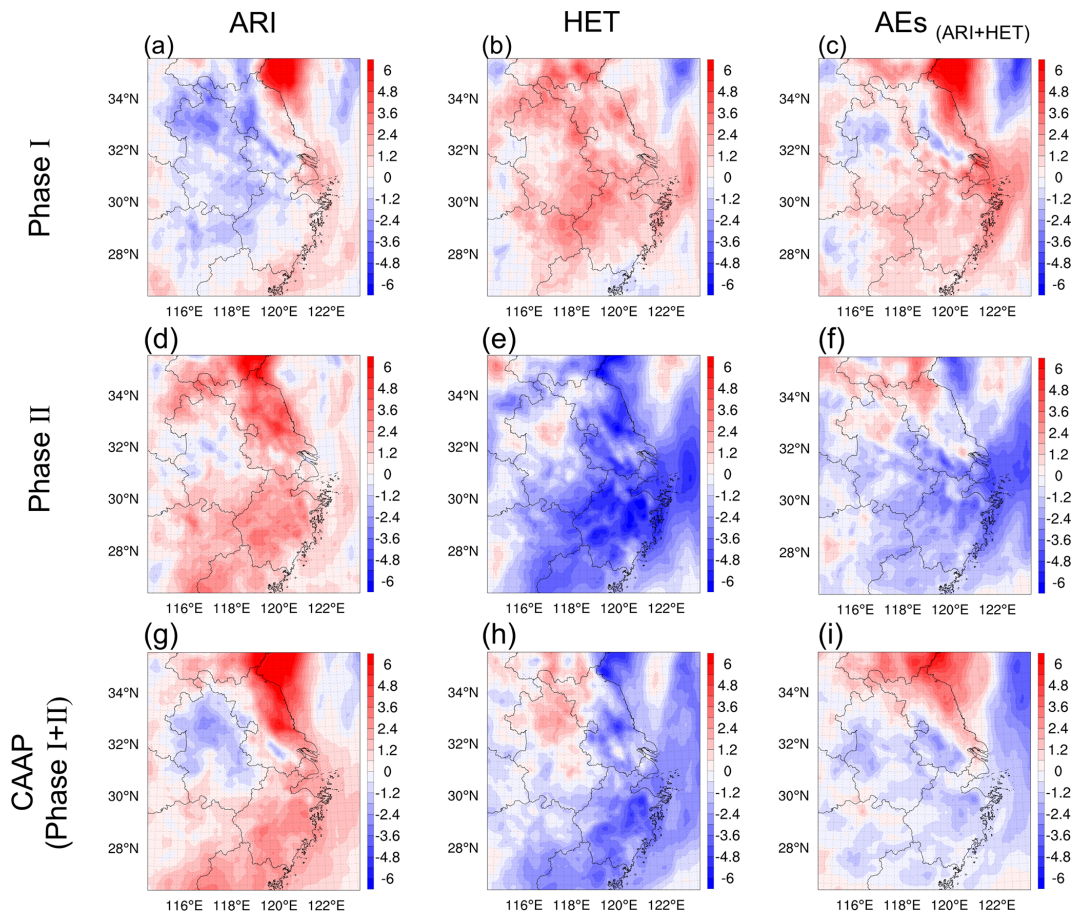


Figure 5. Spatial distribution of summer O₃ changes (ppb) over YRD driven by ARI (a, d, g), HET (b, e, h) and their combined effects (AEs, c, f, i) during two stages of the CAAP.

fect on O₃ between the two phases and underscores the importance of considering the full suite of heterogeneous processes – rather than radical uptake alone – when interpreting aerosol-mediated O₃ responses. In future work, we plan to apply integrated process rate (IPR) diagnostics to more directly evaluate how individual heterogeneous pathways – such as HO₂ uptake, HONO formation, and N₂O₅ hydrolysis – shape the resulting O₃ responses. Coupled with continued improvements in heterogeneous chemistry parameterizations and more comprehensive constraints on radical, reactive nitrogen, and aerosol liquid water fields, this will enable a more detailed and process-resolved understanding of phase-dependent O₃ changes.

To further evaluate whether daytime and nighttime O₃ responses compensate within the daily mean metric, we examined the diurnal cycles of baseline O₃ concentration and the aerosol-mediated impacts (HET, ARI, and AEs) during Phase I, Phase II, and the overall CAAP period for both winter (Fig. S6) and summer (Fig. S7). Across all phases and both seasons, the dominant O₃ perturbations occur during daytime hours, coinciding with the photochemical peak at 14:00–16:00 LT. In winter, Phase I exhibits a

pronounced daytime enhancement driven by ARI (up to ~ 2.41 ppb), whereas HET induces a consistently positive but comparatively weaker increase (up to ~ 0.49 ppb). In Phase II, the ARI-induced enhancement weakens notably (peaking at ~ 1.24 ppb), and HET-induced changes remain minor. In summer, the diurnal behavior more clearly reflects a daytime-dominated response. During Phase I, HET produces a marked midday O₃ enhancement (up to ~ 2.01 ppb), while ARI imposes a weaker yet persistent negative contribution. In contrast, Phase II is characterized by a strong HET-driven daytime O₃ decrease (maximum ~ 3.43 ppb), overwhelming the comparatively modest positive ARI effect. For all cases, nighttime O₃ changes share the same direction as daytime responses but remain substantially smaller in magnitude, insufficient to offset the daytime signals dominated by photochemistry. These diurnal patterns confirm that the phase-dependent O₃ responses to aerosol effects are not artifacts of day–night compensation in daily mean metrics, but instead arise from robust, daytime-dominant photochemical adjustments.

Previous studies showed that ARI and HET were not fully independent and could interact through aerosol–

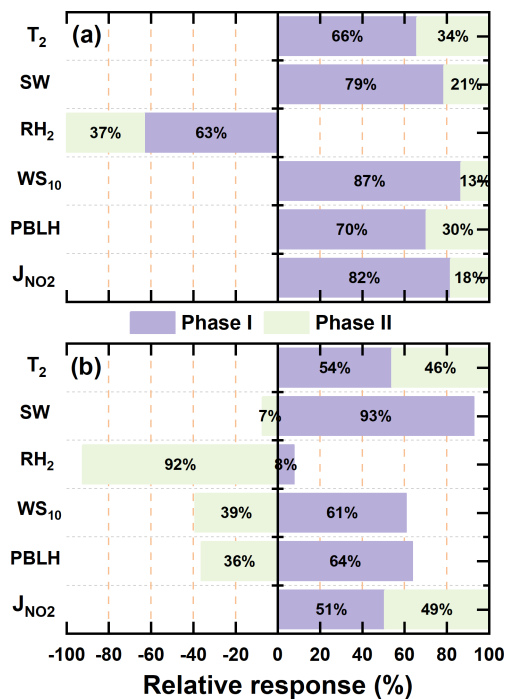


Figure 6. ARI-driven relative responses of meteorological fields and photolysis rates in YRD during winter (a) and summer (b) for the two CAAP stages.

meteorology–chemistry feedbacks (Chen et al., 2019; Liu et al., 2023b; Kong et al., 2018; Li et al., 2020a). ARI-induced increases in near-surface relative humidity typically enhanced aerosol hygroscopic growth and expanded aerosol surface area. The resulting increase in aerosol liquid water promoted gas-to-particle partitioning and facilitated aqueous- and surface-phase reactions, thereby accelerating heterogeneous oxidation pathways involving SO_2 and NO_x . The strengthened heterogeneous formation of secondary inorganic aerosols further modified solar radiation and potentially intensified the ARI effect. In the present study, our primary focus was to quantify the separate and combined contributions of ARI and HET to O_3 changes across different stages of the CAAP. Accordingly, we isolated their individual impacts rather than examining their nonlinear coupling. We acknowledged that ARI–HET interactions might also affect O_3 under certain chemical and meteorological conditions, and we indicated that future work would incorporate dedicated coupled-sensitivity experiments to more explicitly quantify these nonlinearities and their implications for O_3 formation.

Figure S8 illustrated the hierarchical relationships among the four factors analyzed in this section. Emission reductions and meteorological variability constituted the external drivers of O_3 changes, whereas ARI and HET acted as aerosol-mediated modulators that adjust the emission-reduction-driven O_3 responses. This framework motivated

our presentation sequence, where external drivers were examined first, followed by the modulation effects of ARI and HET. Figure 8 presented the relative contributions of major driving factors to surface O_3 changes during the two phases of the CAAP. In winter, anthropogenic emissions emerged as the dominant driver of O_3 increases during Phase I, contributing 6.3 ppb, primarily due to enhanced photochemical production under VOCs-limited conditions. In contrast, Phase II saw a modest O_3 decline (0.9 ppb) resulting from co-reductions in NO_x and VOCs, suggesting improved control effectiveness through coordinated precursor mitigation. Meteorological changes consistently exerted a suppressive effect on wintertime O_3 , contributing -1.7 and -2.1 ppb in Phases I and II, respectively. AEs – mediated by ARI and HET – also contributed to O_3 accumulation, particularly in Phase I (+1.46 ppb), though their influence weakened in Phase II (+0.73 ppb) due to the smaller reductions in aerosol loading. Overall, the wintertime O_3 increase in Phase I was jointly driven by emissions and aerosol-related processes, while the slight decline in Phase II reflected the synergistic benefits of emission reductions and favorable meteorological conditions. In contrast, the attribution profile for summer revealed a dominant role of meteorology. Meteorological variability accounted for a substantial O_3 increase in Phase II (+4.6 ppb), outweighing the contributions of emission changes. The effect of emission reductions on summer O_3 was limited and nonlinear: a slight increase (+1.3 ppb) was observed in Phase I, followed by a minor decline (-1.5 ppb) in Phase II, indicative of a photochemical regime with weak emission sensitivity. Aerosol-related effects exhibited strong seasonal contrasts. HET was the dominant mechanism influencing O_3 in both summer phases, albeit with opposite signs – enhancing O_3 by 1.62 ppb in Phase I but reducing it by 2.86 ppb in Phase II. These contrasting effects likely reflect differences in HO_2 uptake efficiency under evolving humidity and temperature conditions. ARI effects were comparatively modest, leading to a slight O_3 decrease in Phase I (0.51 ppb) and an increase in Phase II (1.56 ppb), likely driven by enhanced photolysis and reduced vertical mixing.

Collectively, these results highlight the evolving interplay among emission control efforts, meteorological conditions, and aerosol effects in shaping surface O_3 trends. While anthropogenic emissions primarily drove winter O_3 increases during the early phase of the CAAP, the roles of meteorology and aerosol processes became increasingly prominent in summer and in the later policy phase. This multi-factor attribution framework aligns well with prior modeling and observational studies in eastern China (Zhu et al., 2021; Zhou et al., 2019). For example, Liu et al. (2023a) demonstrated that declining $\text{PM}_{2.5}$ levels enhanced O_3 formation by weakening HO_2 radical scavenging, particularly under VOCs-limited regimes – a conclusion consistent with our wintertime results. Similarly, Yang et al. (2019) highlighted the growing influence of meteorological variability

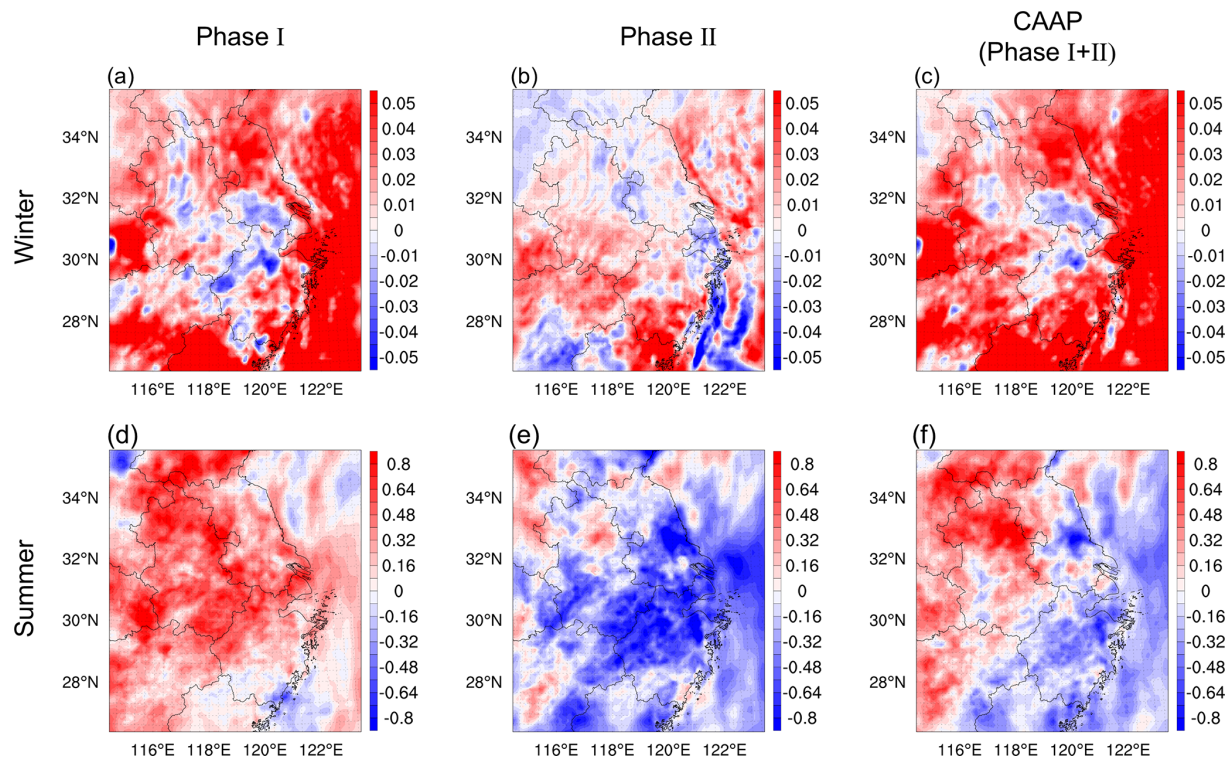


Figure 7. Spatial distributions of HO₂ concentration (ppt) changes induced by HET in winter (a–c) and summer (d–f) during two phases of the CAAP in YRD.

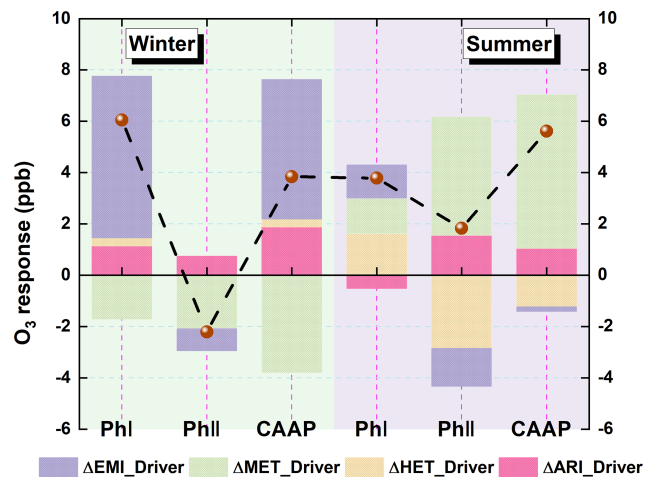


Figure 8. Quantitative attribution of surface O₃ changes over the Yangtze River Delta (YRD) during the two CAAP phases. Contributions from emission reductions (EMI), meteorological variability (MET), aerosol–radiation interactions (ARI), and heterogeneous chemistry (HET) are shown for winter (left) and summer (right).

in recent years as the sensitivity of O₃ to emission changes has diminished. Our study extends this knowledge base by providing phase-resolved attribution and explicitly separating the effects of ARI and HET. Notably, the reversal of HET-driven O₃ responses in summer – from enhancement

to suppression – has rarely been quantified and underscores the importance of dynamically characterizing aerosol–ozone interactions under evolving atmospheric and policy contexts.

3.3 O₃ responses to precursor emission reductions under aerosol effects

Before presenting the simulation results, we first assessed the O₃ chemical regimes over YRD using the widely adopted H₂O₂/HNO₃ ratio (Jeon et al., 2018; Peng et al., 2011; Hammer et al., 2002; Zhang et al., 2000). This metric serves as a diagnostic indicator of O₃ production sensitivity, with ratios < 0.6 indicating VOCs-limited conditions, > 0.8 denoting NO_x-limited regimes, and intermediate values representing transitional states. Figure S9 showed the spatial distribution of this ratio under the baseline scenario (20E20M_AEs). The analysis reveals that wintertime O₃ formation is predominantly VOCs-limited across the YRD, while in summer, most areas exhibit transitional or NO_x-limited regimes, except parts of Anhui Province. Figure 9 displayed the simulated O₃ responses to precursor reductions in both seasons. The results highlight strong seasonal differences and nonlinear sensitivities depending on chemical regime. In winter, reductions in primary PM_{2.5} and NO_x led to substantial O₃ increases. Specifically, 25 % and 50 % reductions in PM_{2.5} increased O₃ by 0.7 and 1.5 ppb, respectively, while NO_x reductions caused even larger enhancements of 4.8 and 10.2 ppb. These

increases primarily stem from weakened aerosol suppression mechanisms – namely reduced heterogeneous uptake and increased photolysis rates – which enhance radical availability and photochemical activity. Additionally, under VOCs-limited conditions, NO_x reductions diminish O_3 titration by NO, further contributing to O_3 accumulation. Among all precursors, NO_x reductions produced the most pronounced O_3 increase. In contrast, NH_3 and SO_2 reductions exerted negligible impacts on O_3 , underscoring their limited roles in direct O_3 photochemistry. VOCs controls, on the other hand, effectively suppressed O_3 formation, with 25 % and 50 % reductions yielding decreases of 2.7 and 5.6 ppb, respectively. In summer, O_3 responses followed broadly similar trends but with different magnitudes. Reducing $\text{PM}_{2.5}$ and NO_x increased O_3 by 2 and 4.3 ppb ($\text{PM}_{2.5}$) and 0.8 and 1.6 ppb (NO_x), respectively. Notably, the O_3 increase associated with $\text{PM}_{2.5}$ reductions exceeded that from NO_x cuts, underscoring the critical role of particulate matter in regulating radical chemistry via aerosol-mediated pathways. VOCs reductions remained the only control strategy that consistently decreased O_3 , lowering concentrations by 1.6 and 3.4 ppb for 25 % and 50 % reductions, respectively. Again, NH_3 and SO_2 reductions had negligible effects. Collectively, these findings suggest that continued $\text{PM}_{2.5}$ -targeted controls may inadvertently worsen O_3 pollution under active AEs, particularly in summer. In contrast, VOCs mitigation remains the most robust and seasonally effective strategy for O_3 reduction.

Figure S10 presented the distribution of O_3 changes under 25 % and 50 % precursor reductions for both seasons. Strong seasonal contrasts and regional gradients in O_3 responses are evident. Reductions in $\text{PM}_{2.5}$ consistently caused widespread O_3 increases across the YRD, with the most pronounced enhancements in northwestern inland regions – particularly southern Jiangsu and central-to-northern Anhui – where historically high aerosol burdens make O_3 formation especially sensitive to weakened aerosol suppression (via ARI and HET). Conversely, coastal cities such as Shanghai and eastern Zhejiang exhibited smaller O_3 increases, reflecting their lower baseline aerosol concentrations and weaker aerosol feedbacks. VOCs reductions led to the largest O_3 decreases in urban corridors, particularly along the Shanghai–Nanjing–Hangzhou (SNH) axis, where VOCs emissions are elevated and O_3 formation is strongly VOCs-sensitive. NO_x reductions yielded seasonally opposite effects: in winter, O_3 increased broadly across the YRD, while in summer, decreases were observed in most regions except Anhui Province. These patterns align with seasonal chemical regimes inferred from $\text{H}_2\text{O}_2/\text{HNO}_3$ ratios – VOCs-limited in winter and NO_x -limited or transitional in summer. NH_3 and SO_2 reductions produced negligible spatial effects in both seasons, reinforcing their limited involvement in direct O_3 photochemistry. These spatially heterogeneous responses highlight the need for geographically differentiated control strategies. Regions with historically high aerosol pollution are more likely to experience unintended O_3 increases following $\text{PM}_{2.5}$ or NO_x

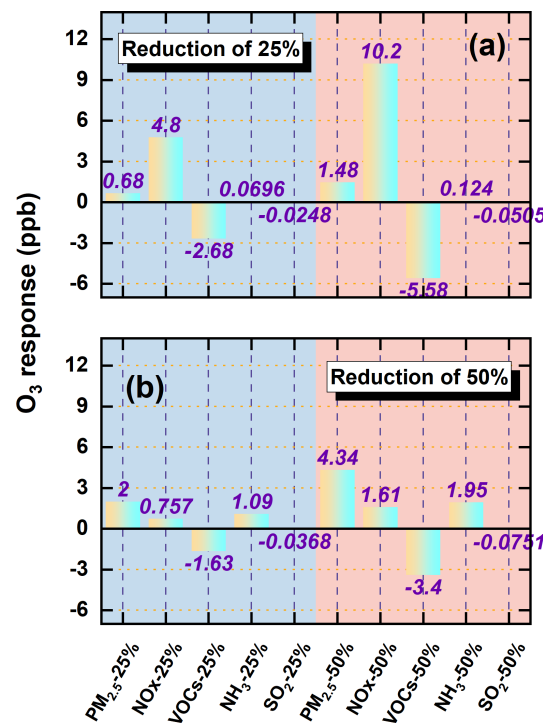


Figure 9. O_3 concentration changes (ppb) in response to 25 % and 50 % reductions in precursor emissions over YRD during winter (a) and summer (b).

reductions. Conversely, VOCs control provides consistent and widespread O_3 benefits across both seasons, making it a key lever for achieving co-benefits in both $\text{PM}_{2.5}$ and O_3 mitigation.

To better understand the temporal dynamics of O_3 responses, we analyzed diurnal variations in four representative cities – Shanghai, Nanjing, Hangzhou, and Hefei – under 50 % reductions of individual precursors (Fig. S11). In winter, NO_x reductions led to substantial O_3 increases during afternoon hours (14:00–17:00 LT (all times are local time)), particularly in urban centers like Shanghai and Hangzhou, where enhancements exceeded 15 ppb. These increases reflect the dual effect of diminished NO titration and enhanced photochemical activity. $\text{PM}_{2.5}$ reductions also caused moderate O_3 increases from late morning to early afternoon, underscoring the influence of both ARI and HET. VOCs reductions induced midday O_3 declines (12:00–15:00) exceeding 5 ppb, consistent with VOCs-limited wintertime chemistry. In summer (Fig. S12), VOCs reductions suppressed O_3 throughout the daytime, with maximum declines reaching up to 25 ppb in early afternoon, reaffirming the effectiveness of VOCs control. In contrast, $\text{PM}_{2.5}$ reductions led to notable O_3 increases during photochemically active hours (11:00–16:00), highlighting the critical role of aerosols in modulating radical cycles and O_3 production. Overall, these diurnal profiles underscore the time-sensitive nature of O_3 responses to precursor emission reductions. They emphasize the necessity

for temporally and spatially refined control strategies that account for local photochemical regimes, emission structures, and AEs.

3.4 Future O₃ responses to Carbon neutrality–driven emission reductions considering aerosol effects

We performed a suite of sensitivity experiments using the 2020 anthropogenic emissions as the baseline to examine prospective O₃ responses to emission mitigation under China's carbon peaking and carbon neutrality pathways. As shown in Fig. 10, O₃ exhibited pronounced seasonal variability in response to progressive emission reductions. In winter, regional mean O₃ increased monotonically with the magnitude of emission cuts, rising from +2.1 % under the 10 % reduction scenario to +14.6 % under the 90 % scenario. This counterintuitive increase is primarily attributed to two synergistic mechanisms: (1) reduced O₃ titration resulting from NO_x emission reductions, and (2) weakened aerosol-mediated O₃ suppression due to lower aerosol loads, which diminish both ARI and HET processes. The reduced availability of aerosol surfaces and optical attenuation enhances photolysis rates and radical propagation, thereby promoting O₃ accumulation. In contrast, summer O₃ declined steadily with increasing emission reductions, from −1.5 % to −16.5 % across the same range. This decline reflects the dominance of VOCs-limited or transitional photochemical regimes in the region during summer, where coordinated reductions in NO_x and VOCs effectively suppress O₃ formation. These results underscore the seasonal asymmetry of O₃ responses under the carbon-neutrality-aligned emission trajectories used in this study – namely the proportional precursor-reduction pathways designed to reflect long-term, economy-wide emission declines. While such stringent reductions may inadvertently aggravate wintertime O₃ pollution, they yield substantial co-benefits for summer O₃ mitigation. The spatial distribution of O₃ changes under these scenarios, presented in Fig. S13, further corroborates the contrasting seasonal patterns. In winter, O₃ increases were most pronounced in inland areas of northern Anhui and central Jiangsu – regions characterized by historically high aerosol burdens and stronger aerosol-mediated O₃ suppression. As emissions decline, the weakening of both aerosol effects and NO_x titration leads to a disproportionate O₃ rebound in these locations. The largest summer O₃ reductions observed in densely populated urban corridors such as Shanghai, Nanjing, and Hangzhou. These metropolitan areas, with high precursor emissions and transitional or NO_x-limited chemical regimes, are particularly responsive to coordinated VOCs and NO_x controls. The spatial heterogeneity in O₃ responses highlights the necessity of designing region-specific and seasonally adaptive emission control strategies. Differentiated approaches are essential given the diverse pollution histories, chemical sensitivities, and aerosol–ozone coupling characteristics across the YRD.

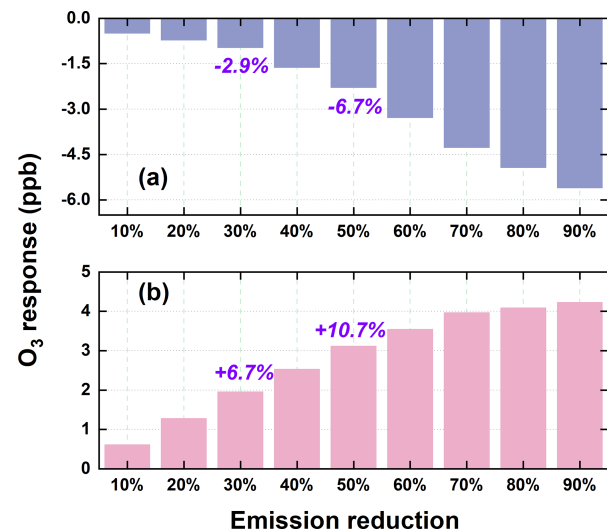


Figure 10. Seasonal variations in O₃ concentrations (ppb) projected under a range of emission reduction intensities (10 %–90 %), including representative scenarios for carbon peaking (30 %) and carbon neutrality (50 %), referenced to 2020 conditions with aerosol-related processes accounted for. Results for summer and winter are displayed in the upper and lower panels, respectively.

Overall, these findings suggest that carbon neutrality–driven emission pathways, if carefully managed, can yield significant summertime O₃ mitigation benefits, but must be complemented with targeted wintertime strategies to avoid adverse trade-offs. The proportional 10 %–90 % reductions applied uniformly across all pollutant species were designed as an idealized framework to systematically examine non-linear O₃ responses under consistent boundary conditions. In practice, however, future emission pathways are expected to exhibit pronounced sectoral and spatial heterogeneity – for example, SO₂ and primary PM_{2.5} typically decline faster than VOCs and NH₃, and the pace of reductions varies across industrial, transportation, and residential sectors. Such differences may influence the magnitude of O₃ responses and the balance among precursor contributions. Recognizing this limitation, future work will incorporate sector-resolved and scenario-specific emission pathways to provide a more realistic assessment of O₃ sensitivity under evolving emission structures.

3.5 Discussion and policy implications

This study presented a comprehensive assessment of O₃ responses to emission reductions under both the CAAP and future carbon neutrality pathways, explicitly considering aerosol effects. Our findings underscore that while emission control measures have been effective in substantially lowering PM_{2.5}, they may yield unintended consequences for O₃ pollution – particularly under VOCs-limited regimes during winter. Specifically, aerosol-induced enhancements in O₃ –

via weakened heterogeneous chemistry (HET) and increased photolysis (ARI) – highlight the necessity of accounting for multiphase feedback mechanisms in the design of future air quality strategies. Our phase-resolved, seasonally differentiated attribution analysis suggests that coordinated reductions in VOCs and NO_x are critical for effective O_3 mitigation, especially in summer when photochemical activity is most intense. Furthermore, the spatial heterogeneity of O_3 responses calls for region-specific strategies. For instance, in inland areas with historically high aerosol burdens, the potential for O_3 rebound due to weakened aerosol suppression is more pronounced, necessitating tailored mitigation approaches. In contrast, urban corridors such as the Shanghai–Nanjing–Hangzhou (SNH) axis – characterized by high VOCs emissions and transitional or NO_x -limited regimes – stand to benefit most from targeted VOCs controls, particularly under future carbon-neutrality-driven reductions.

Uncertainties in HET parameterizations also introduce potential variability into the estimated O_3 responses. The uptake coefficients (γ) for HO_2 , NO_2 , and N_2O_5 depend on aerosol liquid water content, acidity, ionic strength, and particle composition (Jacob, 2000), yet these dependencies remain imperfectly constrained in current atmospheric models. As a result, uncertainties in these parameters may alter the magnitude of individual heterogeneous pathways simulated in this study. For example, higher assumed HO_2 uptake would strengthen radical loss and could reduce the positive HET contribution during Phase I, whereas larger N_2O_5 hydrolysis rates would enhance nighttime conversion of NO_x to HNO_3 and potentially intensify the negative HET influence in Phase II. Likewise, uncertainties in NO_2 uptake and HONO yields could modulate early-morning radical initiation and shift the balance between radical propagation and reactive nitrogen recycling. Importantly, while such uncertainties may influence the absolute magnitude of HET-induced O_3 perturbations, they are unlikely to overturn the direction of the response. Prior modeling studies provide support for this robustness. For instance, Shao et al. (2021) showed that varying γ_{HO_2} between 0.2 and 0.08 altered the magnitude of the O_3 increase driven by reduced HO_2 heterogeneous uptake – from approximately 6 % (consistent with the ~7 % reported by Li et al., 2019a), to about 2.5 % during 2013–2016 – yet the effect remained positive in all cases. These findings indicate that although heterogeneous uptake assumptions can change the amplitude of the response, the sign of the O_3 change is preserved because the underlying chemical mechanism (reduced radical loss leading to enhanced photochemical production) remains the same. By analogy, the phase-dependent sign reversal identified in our study reflects a structural shift in the competition among HO_2 uptake, N_2O_5 hydrolysis, and HONO formation pathways, and is therefore unlikely to be reversed by plausible uncertainties in individual uptake coefficients. Our future studies will incorporate dedicated sensitivity simulations and integrated process rate (IPR) diagnostics to more systemati-

cally quantify how uncertainties in heterogeneous chemistry parameterizations propagate into O_3 simulations. Improvements in observational constraints on aerosol acidity, liquid water content, and heterogeneous reaction rates will further strengthen mechanistic understanding and reduce uncertainty in model-based assessments of aerosol– O_3 interactions under evolving emission pathways.

It is worth emphasizing that all simulations were performed under a fixed-meteorology configuration, which was designed to isolate the influences of aerosol processes and emission changes on O_3 by suppressing interannual meteorological variability. This strategy improves the interpretability of attribution results by reducing confounding weather effects, but it inevitably constrains the model's ability to capture O_3 variability associated with meteorological extremes, such as heat waves or anomalous circulation patterns. As a result, caution is warranted when extending these findings to long-term evolutions or climate-change contexts, where interactions between emissions and meteorology may substantially alter O_3 responses. Future work will explicitly address this limitation by conducting additional sensitivity experiments with time-varying meteorological conditions.

These findings carry timely relevance for China's national climate and environmental goals. As outlined in the 14th Five-Year Plan for Ecological and Environmental Protection and the 2060 Carbon Neutrality Roadmap, deep multi-sector emission cuts are pivotal for achieving synergistic benefits between air quality improvement and climate change mitigation. Our results demonstrate that under prevailing atmospheric chemical regimes – especially during winter – aggressive reductions in primary $\text{PM}_{2.5}$ and NO_x may inadvertently exacerbate O_3 pollution unless accompanied by VOCs-focused controls and regionally tailored strategies. In light of these findings, we advocate for an integrated policy framework that (i) coordinates VOCs and NO_x reductions according to regional O_3 sensitivity, (ii) strengthens VOCs monitoring and inventory resolution at the city level, and (iii) explicitly incorporates aerosol effects in both short-term air pollution forecasting and long-term carbon-neutrality scenarios. Such targeted and mechanism-informed strategies will help bridge the current policy gap between $\text{PM}_{2.5}$ control and O_3 pollution mitigation, while ensuring co-benefits under evolving climate objectives.

4 Conclusions

We employed a phase- and season-specific WRF-Chem framework that explicitly accounted for aerosol–radiation interactions and heterogeneous chemistry to characterize aerosol-driven modulation of O_3 over the YRD from 2013 to 2024. Through combined analyses of emission transitions, meteorological variability, and carbon-neutrality-oriented scenarios, this study provides an integrated assessment of the

mechanisms governing historical O₃ changes and future responses to precursor emission controls.

O₃ exhibited a distinct rise–fall trajectory over the past decade, shaped by complex interactions among emission reductions, meteorological changes, and aerosol effects. During Phase I, substantial reductions in PM_{2.5} and SO₂, coupled with inadequate VOCs controls, led to significant wintertime O₃ increases (6.29 ppb) and modest summer increases (1.28 ppb). In Phase II, more balanced reductions in NO_x and VOCs effectively suppressed O₃ formation. Meteorological variability also exhibited seasonally asymmetric impacts – suppressing O₃ in winter but enhancing accumulation in summer. While wintertime O₃ changes were primarily driven by emissions, summertime variations were dominated by meteorological factors. Aerosol effects further modulated O₃ concentrations through seasonally distinct mechanisms. In winter, ARI played the dominant role: the substantial aerosol reductions in Phase I enhanced solar radiation and boundary layer development, promoting O₃ formation (1.14 ppb); these effects weakened in Phase II (0.73 ppb). Summer O₃ was more sensitive to HET. In Phase I, aerosol decreases weakened heterogeneous radical uptake, enhancing O₃ formation (+1.62 ppb). In Phase II, however, the net HET effect reversed sign (−2.86 ppb), driven by shifts in multiple heterogeneous pathways – including changes in radical uptake, HONO and N₂O₅ chemistry, and aerosol liquid water – rather than radical scavenging alone.

Accounting for aerosol effects, precursor emission reductions elicited marked seasonal and spatial O₃ responses. In winter, a 50 % reduction in VOCs effectively suppressed O₃ by 5.58 ppb, whereas equivalent reductions in NO_x and PM_{2.5} increased O₃ by 10.2 and 1.48 ppb, respectively – primarily due to weakened O₃ titration and radical loss processes. In summer, reductions in PM_{2.5} led to greater increases in O₃ than NO_x (4.34 vs. 1.61 ppb under the 50 % reduction scenario), highlighting the crucial role of aerosol effects in shaping photochemical O₃ production. Under carbon neutrality–driven emission reduction scenarios, O₃ exhibited pronounced seasonally contrasting responses. In winter, O₃ increased monotonically with the magnitude of emission cuts, primarily due to the weakened titration by NO and the diminished aerosol-mediated suppression via heterogeneous chemistry and radiation attenuation. In contrast, summer O₃ consistently declined, with the most substantial improvements observed in high-emission urban corridors. These reductions were mainly driven by the synergistic control of NO_x and VOCs under NO_x-limited and transitional photochemical regimes. When aerosol effects were considered, wintertime O₃ increased by 6.7 % and 10.7 % under carbon peaking and neutrality scenarios, respectively, whereas summertime O₃ decreased by 2.9 % and 6.7 %, highlighting the critical role of multiphase aerosol effects in shaping future air quality outcomes and making climate mitigation strategies.

While this study provides innovative and policy-informative findings, several uncertainties remain that war-

rant further investigation. Uncertainties primarily arise from limitations in the parameterization of heterogeneous chemistry, assumptions in future emission projections, and the current resolution of VOCs emission inventories. Future efforts should prioritize the enhancement of real-time VOCs monitoring, vertical profiling of O₃ and its precursors, and the refinement of multiphase chemical processes in regional models. In conclusion, a holistic and mechanism-informed approach – one that jointly accounts for emissions, aerosol effects, atmospheric chemistry, and meteorology – is essential for the effective co-control of PM_{2.5} and O₃ in the carbon neutrality era. Seasonally adaptive, region-specific, and chemically targeted policies are critical to maximizing air quality and climate co-benefits under evolving environmental and policy contexts.

Code availability. The WRF-Chem model (version 3.7.1) used in this study is based on the standard release from NCAR (<https://doi.org/10.5065/D6MK6B4K>, Grell et al., 2005), with modifications to the aerosol and chemical mechanisms. Details of these modifications are documented in Sect. 2.2 of the paper. The updated code about model and NCL scripts used for data processing and visualization can be provided upon request.

Data availability. The FNL (Final Analysis) meteorological data are available from the Research Data Archive of NCAR: <https://doi.org/10.5065/D6M043C6> (National Centers for Environmental Prediction (NCEP), National Weather Service, U.S. Department of Commerce, 2000). The MEIC v1.4 emission inventory can be accessed at: http://meicmodel.org/?page_id=560 (last access: 20 February 2025). Hourly surface O₃ observations are provided by the China National Environmental Monitoring Centre (CNEMC) and are available at: <http://www.cnemc.cn/> (last access: 26 February 2025).

Supplement. The supplement related to this article is available online at <https://doi.org/10.5194/acp-26-1301-2026-supplement>.

Author contributions. YasL, and TW formulated the research, and YasL: carried it out. ML, YQ, HW, and MX: technical support on the WRF-Chem model. CL, YaoL, and YW: reviewed the manuscript.

Competing interests. The contact author has declared that none of the authors has any competing interests.

Disclaimer. Publisher's note: Copernicus Publications remains neutral with regard to jurisdictional claims made in the text, published maps, institutional affiliations, or any other geographical representation in this paper. The authors bear the ultimate responsibility for providing appropriate place names. Views expressed in the

text are those of the authors and do not necessarily reflect the views of the publisher.

Acknowledgements. We sincerely thank Tsinghua University for providing the anthropogenic emission inventory, and the China National Environmental Monitoring Center for providing the observational datasets. We also extend our heartfelt appreciation to our numerous other institutional collaborators.

Financial support. This investigation was supported by the National Key Basic Research & Development Program of China (grant no. 2024YFC3711905), the Doctoral Scientific Research Fund of Henan Finance University (grant no. 2024BS055), and the National Natural Science Foundation of China (grant no. 42477103), the Creative talent exchange program for foreign experts in the Belt and Road countries, the Henan Provincial Science and Technology Research and Development Program (grant no. 252102320085).

Review statement. This paper was edited by Carl Percival and reviewed by two anonymous referees.

References

Brown, S. S. and Stutz, J.: Nighttime radical observations and chemistry, *Chem. Soc. Rev.*, 41, 6405–6447, <https://doi.org/10.1039/C2CS35181A>, 2012.

Cao, J., Qiu, X., Liu, Y., Yan, X., Gao, J., and Peng, L.: Identifying the dominant driver of elevated surface ozone concentration in North China plain during summertime 2012–2017, *Environ. Pollut.*, 300, 118912, <https://doi.org/10.1016/j.envpol.2022.118912>, 2022.

Chen, J., Li, Z., Lv, M., Wang, Y., Wang, W., Zhang, Y., Wang, H., Yan, X., Sun, Y., and Cribb, M.: Aerosol hygroscopic growth, contributing factors, and impact on haze events in a severely polluted region in northern China, *Atmos. Chem. Phys.*, 19, 1327–1342, <https://doi.org/10.5194/acp-19-1327-2019>, 2019.

Chen, X., Zhong, B., Huang, F., Wang, X., Sarkar, S., Jia, S., Deng, X., Chen, D., and Shao, M.: The role of natural factors in constraining long-term tropospheric ozone trends over Southern China, *Atmos. Environ.*, 220, 117060, <https://doi.org/10.1016/j.atmosenv.2019.117060>, 2020.

Cheng, J., Tong, D., Zhang, Q., Liu, Y., Lei, Y., Yan, G., Yan, L., Yu, S., Cui, R. Y., Clarke, L., Geng, G., Zheng, B., Zhang, X., Davis, S. J., and He, K.: Pathways of China's PM_{2.5} air quality 2015–2060 in the context of carbon neutrality, *Natl. Sci. Rev.*, 8, <https://doi.org/10.1093/nsr/nwab078>, 2021.

Dai, H., Liao, H., Li, K., Yue, X., Yang, Y., Zhu, J., Jin, J., Li, B., and Jiang, X.: Composited analyses of the chemical and physical characteristics of co-polluted days by ozone and PM_{2.5} over 2013–2020 in the Beijing–Tianjin–Hebei region, *Atmos. Chem. Phys.*, 23, 23–39, <https://doi.org/10.5194/acp-23-23-2023>, 2023.

Dai, H., Liao, H., Wang, Y., and Qian, J.: Co-occurrence of ozone and PM_{2.5} pollution in urban/non-urban areas in eastern China from 2013 to 2020: Roles of meteorology and anthropogenic emissions, *Sci. Total Environ.*, 924, 171687, <https://doi.org/10.1016/j.scitotenv.2024.171687>, 2024.

Dang, R., Liao, H., and Fu, Y.: Quantifying the anthropogenic and meteorological influences on summertime surface ozone in China over 2012–2017, *Sci. Total Environ.*, 754, 142394, <https://doi.org/10.1016/j.scitotenv.2020.142394>, 2021.

Dyson, J. E., Whalley, L. K., Slater, E. J., Woodward-Massey, R., Ye, C., Lee, J. D., Squires, F., Hopkins, J. R., Dunmore, R. E., Shaw, M., Hamilton, J. F., Lewis, A. C., Worrall, S. D., Bacak, A., Mehra, A., Bannan, T. J., Coe, H., Percival, C. J., Ouyang, B., Hewitt, C. N., Jones, R. L., Crilley, L. R., Kramer, L. J., Acton, W. J. F., Bloss, W. J., Saksakulkrai, S., Xu, J., Shi, Z., Harrison, R. M., Kotthaus, S., Grimmond, S., Sun, Y., Xu, W., Yue, S., Wei, L., Fu, P., Wang, X., Arnold, S. R., and Heard, D. E.: Impact of HO₂ aerosol uptake on radical levels and O₃ production during summertime in Beijing, *Atmos. Chem. Phys.*, 23, 5679–5697, <https://doi.org/10.5194/acp-23-5679-2023>, 2023.

Gao, J., Zhu, B., Xiao, H., Kang, H., Pan, C., Wang, D., and Wang, H.: Effects of black carbon and boundary layer interaction on surface ozone in Nanjing, China, *Atmos. Chem. Phys.*, 18, 7081–7094, <https://doi.org/10.5194/acp-18-7081-2018>, 2018.

Geng, G., Liu, Y., Liu, Y., Liu, S., Cheng, J., Yan, L., Wu, N., Hu, H., Tong, D., and Zheng, B.: Efficacy of China's clean air actions to tackle PM_{2.5} pollution between 2013 and 2020, *Nat. Geosci.*, 17, 987–994, <https://doi.org/10.1038/s41561-024-01540-z>, 2024.

George, C., Ammann, M., D'Anna, B., Donaldson, D. J., and Nizkorodov, S. A.: Heterogeneous Photochemistry in the Atmosphere, *Chem. Rev.*, 115, 4218–4258, <https://doi.org/10.1021/cr500648z>, 2015.

Grell, G. A., Peckham, S. E., Schmitz, R., McKeen, S. A., Frost, G., Skamarock, W. C., and Eder, B.: Fully coupled “online” chemistry within the WRF model, *Atmos. Environ.*, 39, 6957–6975, <https://doi.org/10.1016/j.atmosenv.2005.04.027>, 2005.

Guenther, A., Karl, T., Harley, P., Wiedinmyer, C., Palmer, P. I., and Geron, C.: Estimates of global terrestrial isoprene emissions using MEGAN (Model of Emissions of Gases and Aerosols from Nature), *Atmos. Chem. Phys.*, 6, 3181–3210, <https://doi.org/10.5194/acp-6-3181-2006>, 2006.

Hammer, M. U., Vogel, B., and Vogel, H.: Findings on H₂O₂/HNO₃ as an indicator of ozone sensitivity in Baden-Württemberg, Berlin-Brandenburg, and the Po valley based on numerical simulations, *J. Geophys. Res.: Atmos.*, 107, LOP 3-1–LOP 3-18, <https://doi.org/10.1029/2000JD000211>, 2002.

Hu, F., Xie, P., Xu, J., Lv, Y., Zhang, Z., Zheng, J., and Tian, X.: Long-term trends of ozone in the Yangtze River Delta, China: spatiotemporal impacts of meteorological factors, local, and non-local emissions, *J. Environ. Sci.*, 156, 408–420, <https://doi.org/10.1016/j.jes.2024.07.017>, 2025.

Jacob, D. J.: Heterogeneous chemistry and tropospheric ozone, *Atmos. Environ.*, 34, 2131–2159, [https://doi.org/10.1016/S1352-2310\(99\)00462-8](https://doi.org/10.1016/S1352-2310(99)00462-8), 2000.

Jeon, W., Choi, Y., Souri, A. H., Roy, A., Diao, L., Pan, S., Lee, H. W., and Lee, S.-H.: Identification of chemical fingerprints in long-range transport of burning induced upper tropospheric ozone from Colorado to the North Atlantic Ocean, *Sci. Total Environ.*, 613–614, 820–828, <https://doi.org/10.1016/j.scitotenv.2017.09.177>, 2018.

Kong, L., Du, C., Zhanzakova, A., Cheng, T., Yang, X., Wang, L., Fu, H., Chen, J., and Zhang, S.: Trends in heterogeneous aqueous reaction in continuous haze episodes in suburban Shanghai: An in-depth case study, *Sci. Total Environ.*, 634, 1192–1204, <https://doi.org/10.1016/j.scitotenv.2018.04.086>, 2018.

Li, J., Han, Z., Li, J., Liu, R., Wu, Y., Liang, L., and Zhang, R.: The formation and evolution of secondary organic aerosol during haze events in Beijing in wintertime, *Sci. Total Environ.*, 703, 134937, <https://doi.org/10.1016/j.scitotenv.2019.134937>, 2020a.

Li, K., Jacob, D. J., Liao, H., Shen, L., Zhang, Q., and Bates, K. H.: Anthropogenic drivers of 2013–2017 trends in summer surface ozone in China, *Proceedings of the National Academy of Sciences*, 116, 422–427, <https://doi.org/10.1073/pnas.1812168116>, 2019a.

Li, K., Jacob, D. J., Shen, L., Lu, X., De Smedt, I., and Liao, H.: Increases in surface ozone pollution in China from 2013 to 2019: anthropogenic and meteorological influences, *Atmos. Chem. Phys.*, 20, 11423–11433, <https://doi.org/10.5194/acp-20-11423-2020>, 2020b.

Li, M., Wang, T., Xie, M., Li, S., Zhuang, B., Chen, P., Huang, X., and Han, Y.: Agricultural Fire Impacts on Ozone Photochemistry Over the Yangtze River Delta Region, East China, *J. Geophys. Res.: Atmos.*, 123, 6605–6623, <https://doi.org/10.1029/2018JD028582>, 2018.

Li, M., Zhang, Q., Zheng, B., Tong, D., Lei, Y., Liu, F., Hong, C., Kang, S., Yan, L., Zhang, Y., Bo, Y., Su, H., Cheng, Y., and He, K.: Persistent growth of anthropogenic non-methane volatile organic compound (NMVOC) emissions in China during 1990–2017: drivers, speciation and ozone formation potential, *Atmos. Chem. Phys.*, 19, 8897–8913, <https://doi.org/10.5194/acp-19-8897-2019>, 2019b.

Li, Y., Wang, T., Wang, Q. G., Qu, Y., Wu, H., Xie, M., Li, M., Li, S., and Zhuang, B.: Spatiotemporal Variations of PM_{2.5} and O₃ Relationship during 2014–2021 in Eastern China, *Aerosol and Air Quality Research*, 23, 230060, <https://doi.org/10.4209/aaqr.230060>, 2023.

Li, Y., Wang, T., Wang, Q. G., Li, M., Qu, Y., Wu, H., and Xie, M.: Exploring the role of aerosol-ozone interactions on O₃ surge and PM_{2.5} decline during the clean air action period in Eastern China 2014–2020, *Atmos. Res.*, 302, 107294, <https://doi.org/10.1016/j.atmosres.2024.107294>, 2024a.

Li, Y., Wang, T., Wang, Q. G., Li, M., Qu, Y., Wu, H., Fan, J., Shao, M., and Xie, M.: Deciphering the seasonal dynamics of multifaceted aerosol-ozone interplay: Implications for air quality management in Eastern China, *Sci. Total Environ.*, 946, 174327, <https://doi.org/10.1016/j.scitotenv.2024.174327>, 2024b.

Li, Y., Wang, T., Wang, Q. G., Li, M., Qu, Y., Wu, H., and Xie, M.: Impact of aerosol-radiation interaction and heterogeneous chemistry on the winter decreasing PM_{2.5} and increasing O₃ in Eastern China 2014–2020, *J. Environ. Sci.*, 151, 469–483, <https://doi.org/10.1016/j.jes.2024.04.010>, 2025.

Liu, H., Liu, S., Xue, B., Lv, Z., Meng, Z., Yang, X., Xue, T., Yu, Q., and He, K.: Ground-level ozone pollution and its health impacts in China, *Atmos. Environ.*, 173, 223–230, <https://doi.org/10.1016/j.atmosenv.2017.11.014>, 2018.

Liu, Y. and Wang, T.: Worsening urban ozone pollution in China from 2013 to 2017 – Part 1: The complex and varying roles of meteorology, *Atmos. Chem. Phys.*, 20, 6305–6321, <https://doi.org/10.5194/acp-20-6305-2020>, 2020.

Liu, Y., Geng, G., Cheng, J., Liu, Y., Xiao, Q., Liu, L., Shi, Q., Tong, D., He, K., and Zhang, Q.: Drivers of Increasing Ozone during the Two Phases of Clean Air Actions in China 2013–2020, *Environ. Sci. Technol.*, 57, 8954–8964, <https://doi.org/10.1021/acs.est.3c00054>, 2023a.

Liu, Z., Wang, H., Peng, Y., Zhang, W., Che, H., Zhang, Y., Liu, H., Wang, Y., Zhao, M., and Zhang, X.: The combined effects of heterogeneous chemistry and aerosol-radiation interaction on severe haze simulation by atmospheric chemistry model in Middle-Eastern China, *Atmos. Environ.*, 302, 119729, <https://doi.org/10.1016/j.atmosenv.2023.119729>, 2023b.

Lu, S., Gong, S., Chen, J., Zhang, L., Ke, H., Pan, W., Lu, J., and You, Y.: Contribution assessment of meteorology vs. emissions in the summer ozone trend from 2014 to 2023 in China by an environmental meteorology index, *Atmos. Environ.*, 343, 120992, <https://doi.org/10.1016/j.atmosenv.2024.120992>, 2025.

Ma, D., Wang, T., Wu, H., Qu, Y., Liu, J., Liu, J., Li, S., Zhuang, B., Li, M., and Xie, M.: The effect of anthropogenic emission, meteorological factors, and carbon dioxide on the surface ozone increase in China from 2008 to 2018 during the East Asia summer monsoon season, *Atmos. Chem. Phys.*, 23, 6525–6544, <https://doi.org/10.5194/acp-23-6525-2023>, 2023a.

Ma, P., Quan, J., Dou, Y., Pan, Y., Liao, Z., Cheng, Z., Jia, X., Wang, Q., Zhan, J., Ma, W., Zheng, F., Wang, Y., Zhang, Y., Hua, C., Yan, C., Kulmala, M., Liu, Y., Huang, X., Yuan, B., Brown, S. S., and Liu, Y.: Regime-Dependence of Nocturnal Nitrate Formation via N₂O₅ Hydrolysis and Its Implication for Mitigating Nitrate Pollution, *Geophys. Res. Lett.*, 50, e2023GL106183, <https://doi.org/10.1029/2023GL106183>, 2023b.

National Centers for Environmental Prediction (NCEP), National Weather Service, U.S. Department of Commerce: NCEP FNL Operational Model Global Tropospheric Analyses, continuing from July 1999, NSF National Center for Atmospheric Research [data set], <https://doi.org/10.5065/D6M043C6>, 2000.

Ni, Y., Yang, Y., Wang, H., Li, H., Li, M., Wang, P., Li, K., and Liao, H.: Contrasting changes in ozone during 2019–2021 between eastern and the other regions of China attributed to anthropogenic emissions and meteorological conditions, *Sci. Total Environ.*, 908, 168272, <https://doi.org/10.1016/j.scitotenv.2023.168272>, 2024.

Peng, Y.-P., Chen, K.-S., Wang, H.-K., Lai, C.-H., Lin, M.-H., and Lee, C.-H.: Applying model simulation and photochemical indicators to evaluate ozone sensitivity in southern Taiwan, *J. Environ. Sci.*, 23, 790–797, [https://doi.org/10.1016/S1001-0742\(10\)60479-2](https://doi.org/10.1016/S1001-0742(10)60479-2), 2011.

Qu, Y., Wang, T., Yuan, C., Wu, H., Gao, L., Huang, C., Li, Y., Li, M., and Xie, M.: The underlying mechanisms of PM_{2.5} and O₃ synergistic pollution in East China: Photochemical and heterogeneous interactions, *Sci. Total Environ.*, 873, 162434, <https://doi.org/10.1016/j.scitotenv.2023.162434>, 2023.

Shao, M., Wang, W., Yuan, B., Parrish, D. D., Li, X., Lu, K., Wu, L., Wang, X., Mo, Z., Yang, S., Peng, Y., Kuang, Y., Chen, W., Hu, M., Zeng, L., Su, H., Cheng, Y., Zheng, J., and Zhang, Y.: Quantifying the role of PM_{2.5} dropping in variations of ground-level ozone: Inter-comparison between Beijing and Los Angeles, *Sci. Total Environ.*, 788, 147712, <https://doi.org/10.1016/j.scitotenv.2021.147712>, 2021.

Shao, M., Lv, S., Song, Y., Liu, R., and Dai, Q.: Disentangling the effects of meteorology and emissions from

anthropogenic and biogenic sources on the increased surface ozone in Eastern China, *Atmos. Res.*, 311, 107699, <https://doi.org/10.1016/j.atmosres.2024.107699>, 2024.

Sun, L., Xue, L., Wang, Y., Li, L., Lin, J., Ni, R., Yan, Y., Chen, L., Li, J., Zhang, Q., and Wang, W.: Impacts of meteorology and emissions on summertime surface ozone increases over central eastern China between 2003 and 2015, *Atmos. Chem. Phys.*, 19, 1455–1469, <https://doi.org/10.5194/acp-19-1455-2019>, 2019.

Wu, K., Wang, Y., Qiao, Y., Liu, Y., Wang, S., Yang, X., Wang, H., Lu, Y., Zhang, X., and Lei, Y.: Drivers of 2013–2020 ozone trends in the Sichuan Basin, China: Impacts of meteorology and precursor emission changes, *Environ. Pollut.*, 300, 118914, <https://doi.org/10.1016/j.envpol.2022.118914>, 2022.

Yan, D., Jin, Z., Zhou, Y., Li, M., Zhang, Z., Wang, T., Zhuang, B., Li, S., and Xie, M.: Anthropogenically and meteorologically modulated summertime ozone trends and their health implications since China's clean air actions, *Environ. Pollut.*, 343, 123234, <https://doi.org/10.1016/j.envpol.2023.123234>, 2024.

Yang, H., Chen, L., Liao, H., Zhu, J., Wang, W., and Li, X.: Weakened aerosol–radiation interaction exacerbating ozone pollution in eastern China since China's clean air actions, *Atmos. Chem. Phys.*, 24, 4001–4015, <https://doi.org/10.5194/acp-24-4001-2024>, 2024.

Yang, L., Luo, H., Yuan, Z., Zheng, J., Huang, Z., Li, C., Lin, X., Louie, P. K. K., Chen, D., and Bian, Y.: Quantitative impacts of meteorology and precursor emission changes on the long-term trend of ambient ozone over the Pearl River Delta, China, and implications for ozone control strategy, *Atmos. Chem. Phys.*, 19, 12901–12916, <https://doi.org/10.5194/acp-19-12901-2019>, 2019.

Yin, H., Lu, X., Sun, Y., Li, K., Gao, M., Zheng, B., and Liu, C.: Unprecedented decline in summertime surface ozone over eastern China in 2020 comparably attributable to anthropogenic emission reductions and meteorology, *Environ. Res. Lett.*, 16, 124069, <https://doi.org/10.1088/1748-9326/ac3e22>, 2021.

Yu, C., Huang, L., Xue, L., Shen, H., Li, Z., Zhao, M., Yang, J., Zhang, Y., Li, H., Mu, J., and Wang, W.: Photoenhanced Heterogeneous Uptake of NO₂ and HONO Formation on Authentic Winter Time Urban Grime, *ACS Earth Space Chem.*, 6, 1960–1968, <https://doi.org/10.1021/acsearthspacechem.2c00054>, 2022.

Yu, Y., Wang, Z., He, T., Meng, X., Xie, S., and Yu, H.: Driving factors of the significant increase in surface ozone in the Yangtze River Delta, China, during 2013–2017, *Atmos. Pollut. Res.*, 10, 1357–1364, <https://doi.org/10.1016/j.apr.2019.03.010>, 2019.

Zhai, S., Jacob, D. J., Wang, X., Shen, L., Li, K., Zhang, Y., Gui, K., Zhao, T., and Liao, H.: Fine particulate matter (PM_{2.5}) trends in China, 2013–2018: separating contributions from anthropogenic emissions and meteorology, *Atmos. Chem. Phys.*, 19, 11031–11041, <https://doi.org/10.5194/acp-19-11031-2019>, 2019.

Zhang, H., Roehl, C. M., Sander, S. P., and Wennberg, P. O.: Intensity of the second and third OH overtones of H₂O₂, HNO₃, and HO₂NO₂, *J. Geophys. Res.: Atmos.*, 105, 14593–14598, <https://doi.org/10.1029/2000JD900118>, 2000.

Zhang, X., Zhang, W.-C., Wu, W., and Liu, H.-B.: Understanding ozone variability in spatial responses to emissions and meteorology in China using interpretable machine learning, *iScience*, 28, 113036, <https://doi.org/10.1016/j.isci.2025.113036>, 2025.

Zhao, X., Zhang, Z., Xu, J., Gao, J., Cheng, S., Zhao, X., Xia, X., and Hu, B.: Impacts of aerosol direct effects on PM_{2.5} and O₃ respond to the reductions of different primary emissions in Beijing-Tianjin-Hebei and surrounding area, *Atmos. Environ.*, 309, 119948, <https://doi.org/10.1016/j.atmosenv.2023.119948>, 2023.

Zhou, M., Zhang, L., Chen, D., Gu, Y., Fu, T.-M., Gao, M., Zhao, Y., Lu, X., and Zhao, B.: The impact of aerosol–radiation interactions on the effectiveness of emission control measures, *Environ. Res. Lett.*, 14, 024002, <https://doi.org/10.1088/1748-9326/aaf27d>, 2019.

Zhu, J., Chen, L., Liao, H., Yang, H., Yang, Y., and Yue, X.: Enhanced PM_{2.5} Decreases and O₃ Increases in China During COVID-19 Lockdown by Aerosol-Radiation Feedback, *Geophys. Res. Lett.*, 48, e2020GL090260, <https://doi.org/10.1029/2020GL090260>, 2021.